# Collisional excitation of CH($X^2\Pi$) by He: New *ab initio* potential energy surfaces and scattering calculations

Sarantos Marinakis*
*Department of Chemistry and Biochemistry, School of Biological and Chemical Sciences, Queen Mary University of London, Joseph Priestley Building, Mile End Road, London E1 4NS, UK*

Indigo Lily Dean†
*Department of Chemistry and Biochemistry, School of Biological and Chemical Sciences, Queen Mary University of London, Joseph Priestley Building, Mile End Road, London E1 4NS, UK*

Jacek Kłos‡
*Department of Chemistry and Biochemistry, University of Maryland, College Park, Maryland 20742-2021, USA*

François Lique§
*LOMC - UMR 6294, CNRS-Université du Havre, 25 rue Philippe Lebon, BP 1123 - 76 063 Le Havre cedex, France*

(Dated: July 15, 2015)

We present a new set of potential energy surfaces (PESs) for the CH($X^2\Pi$)–He van der Waals system. *Ab initio* calculations of the CH–He PES were carried out using the open-shell single- and double-excitation coupled cluster approach with non-iterative perturbational treatment of triple excitations [RCCSD(T)]. The augmented correlation-consistent polarized valence quadruple-zeta aug-cc-pVQZ basis set was employed augmented by mid-bond functions. Integral cross sections for the rotational excitation in CH–He collisions were calculated using the new PES and compared with available experimental results. The newly constructed PES reproduces the available experimental results for CH($X^2\Pi, v = 0$)–He collisions better than any previously available PES. Differential cross sections (DCS) are presented for the first time for this system and discussed within the context of rotational rainbows. Finally, our work provides the first rate thermal coefficients for this system that are crucially needed for astrochemical modelling and future anticipated experiments in CH($X^2\Pi, v = 0$)–He collisions.

## I. INTRODUCTION

The methylidene (CH) radical plays a significant role in hydrocarbon combustion reactions [1], in the interstellar medium (ISM) [2], in the sun and stellar atmospheres [3, 4] and in comets [5]. It was one of the first molecules to be observed in the ISM, and it is one of the most abundant diatomic species in molecular clouds. CH became a common probe of the diffuse interstellar medium. The launch of the Herschel Space Observatory in 2010 opened a spectral domain hidden by the opacity of the Earth atmosphere so that the Herschel satellite have recently collected new CH emission data [6–8] with a spectral resolution previously unmatched. This makes CH an excellent tracer of the gas density in diffuse as well as translucent-to-denser molecular clouds [8].

Together with radiative field emitted by stars, collisions of CH(X) with H, $H_2$, He and electrons are expected to be responsible for the CH(X) rovibrational populations observed in astrophysical media. The methylidene being a small hydrocarbon radical is also of interest in flame modelling and its transport coefficients in helium can be calculated using the new more accurate potentials presented in this work. From a theoretical point of view, CH(X)–He collisions are much simpler than the reactive CH(X) + $H/H_2$ collisions and as such they have attracted much theoretical and experimental work.

The methylidene radical is also a very useful diatomic in the search for varying fundamental constants. Because of this, Truppe *et al.* presented the most accurate frequencies of CH microwave [9, 10] and millimeter [11] transitions.

The ground electronic state configuration of CH is $1\sigma^2 2\sigma^2 3\sigma^2 1\pi^1$, and therefore the ground electronic state is of $^2\Pi$ symmetry [12]. The methylidene is a Hund's case (b) radical in its lowest rovibrational levels in its ground electronic state, with the $^2\Pi_{1/2}$ spin-orbit state being lower than the $^2\Pi_{3/2}$ [13]. The $^2\Pi_{1/2}$ and $^2\Pi_{3/2}$ are labeled $F_2$ and $F_1$, respectively. The electronic orbital angular momentum, **L**, is coupled with the rotational angular momentum of the bare nuclei, **R**, to form the total (excluding nuclear and electron spin) angular momentum, **N**. **N** is then coupled with the electron spin angular momentum, **S**, giving the total angular momentum, **J**. In Hund's case (b), $J = N \pm 1/2$ for the $F_1$ and $F_2$ manifolds, respectively. **J** is coupled with the nuclear spin of H ($I = 1/2$) to give the grand total angular momentum, **F**.

* s.marinakis@qmul.ac.uk
† i.dean@se12.qmul.ac.uk
‡ jklos@umd.edu
§ francois.lique@univ-lehavre.fr

Each rotational level is split into two Λ-doublet levels of opposite parity. Collisional and photodissociation processes often lead to a selective population of these levels. These 'propensity' rules arise due to the different properties, i.e. parity and symmetry of these nearly degenerate Λ-doublet levels. The labelling of Λ-doublet levels in diatomic molecules employs the symbols $e/f$ for the parity [14], and the symbols $A'/A''$ for the symmetry [15]. In the case of CH, the total number of electrons is odd and therefore the total angular momentum quantum number, $J$, is half-integer. When the sign of the wave function of a given level remains the same under space-fixed inversion operator, the level has a positive parity, $p = +1$. Levels with parity $(-1)^{J-1/2}$ or $-(-1)^{J-1/2}$ are designated as $e$ or $f$, respectively. All series of levels in which the electronic wave function at high $J$ is symmetric or antisymmetric with respect to reflection of the spatial coordinates of the electrons in the plane of rotation are designated as $A'$ or $A''$, respectively. In CH(X), the $F_1e$ and $F_2f$ are $A'$, and the $F_1f$ and $F_2e$ are $A''$.

The interaction of CH(X) with any rare gas atom can be described using two adiabatic potential energy surfaces (PES), $^2A'$ and $^2A''$. The former PES describes the He-CH system when the singly occupied orbital lies in the He-C-H plane. The $^2A''$ PES describes the He-CH system when the radical orbital is perpendicular to that plane. In the scattering calculations, it is more convenient [16] to use the average $V_{\rm sum} = \frac{1}{2}\left(V_{A''} + V_{A'}\right)$, and the half-difference $V_{\rm diff} = \frac{1}{2}\left(V_{A''} - V_{A'}\right)$ of these two PESs (as defined later on in Eqs. 3 and 4), respectively. The intermolecular potential can be conveniently expressed in Jacobi coordinates $(R, \theta, r)$, where $R$ is the distance between the CH centre of mass and the He atom, $\theta$ is the Jacobi angle between the intermolecular vector, $\mathbf{R}$, and the CH bond vector, $\mathbf{r}$.

Macdonald and Liu [17] presented the first, and only so far, experimental work on CH(X)–He collisions

$$\mathrm{CH}(X^2\Pi, N, J, \varepsilon) + \mathrm{He} \rightarrow \mathrm{CH}(X^2\Pi', N', J', \varepsilon') + \mathrm{He} \quad (1)$$

where $\varepsilon$ and $\varepsilon'$ can be either $e$ or $f$. Using supersonic expansion, they were able to state-select CH(X) radicals in the lowest rotational levels and with equal population in the Λ-doublet components. In their crossed-beam experiment, the CH(X) radicals collided with He atoms at collision energies ($E_{\rm col}$) between 150 and 1400 $\mathrm{cm}^{-1}$. The product CH($N'$ = 3-7) levels were then probed in a state-specific manner using laser-induced fluorescence (LIF). Macdonald and Liu were able to obtain relative values of inelastic integral cross sections, and they observed a clear propensity for population of $\Pi(A'')$ final levels in rotational excitation of CH(X) radicals.

Dagdigian *et al.* [18] explained this propensity using a rather powerful argument which did not require any accurate values of the underlying PES. They described the interaction between any $\pi^1$ (or $\pi^3$) diatomic radical and a rare gas atom in terms of $V_{\rm sum}$ and $V_{\rm diff}$. They went on to expand $V_{\rm sum}$ as a sum of $P_l(\cos(\theta)V_{l0}(R)$, and $V_{\rm diff}$ as a sum of $P_l^2(\cos(\theta)V_{l2}(R)$, where $P_l$ and $P_l^2$ are the regular and associated Legendre polynomials, respectively. They argued that in the case of CH(X)–He $A''$ PES, the $\pi^1$ radical orbital is out of the plane, which allows a very close approach of the collision partner in the direction perpendicular to the bond. The average potential is mainly repulsive and hence has a positive sign, while the difference potential is predominantly negative. By expanding the potential matrix elements in terms of $V_{l0}(R)$ and $V_{l2}(R)$, they showed that when the $V_{l2}(R)$ terms are of opposite sign to the corresponding $V_{l0}(R)$ terms, something expected to be true for $\pi^1$ radicals, then upward transitions into $\Pi(A'')$ levels will be favoured compared with transitions into $\Pi(A')$ levels. They also used the PES by Wagner *et al.*, which was unpublished at the time, in order to obtain values of integral cross sections, which were in qualitative agreement with the experimental measurements at a collision energy of 1000 $\mathrm{cm}^{-1}$.

Five years later, the first *ab initio* study of He-CH(X) was presented by Wagner *et al.* [19]. They confirmed that the $^2A'$ and $^2A''$ adiabatic PESs have very different characteristics, with the former PES being more repulsive than the latter at bent geometries. The $^2A'$ PES had a shallow minimum corresponding to a collinear configuration, while the $^2A''$ showed a much deeper minimum corresponding to a T-shaped arrangement. Alexander *et al.* [20] used those PESs and obtained close-coupling quantum mechanical integral cross sections which were in a generally good agreement with the experimental values obtained by Macdonald and Liu [17].

Cybulski *et al.* [21] used unrestricted Møller-Plesset perturbation theory to obtain PESs that had similar shapes with those by Wagner *et al.* but contrasting numerical values. Later on, Ben Abdallah *et al.* [22] obtained a well depth of the $^2A''$ potential, $D_{\rm e}$, of 60 $\mathrm{cm}^{-1}$ at $R = 5.2\,a_0$ and $\theta = 80°$ using coupled electron pair approximation (CEPA-1) and augmented correlation-consistent polarized valence quadruple-zeta aug-cc-pVQZ (aVQZ) basis set. The minimum was much deeper than the previously calculated values of 15.8 $\mathrm{cm}^{-1}$ and 47 $\mathrm{cm}^{-1}$ reported by Wagner *et al.* [19] and Cybulski *et al.* [21], respectively. Ben Abdallah *et al.* were also able to observe a second minimum in the $^2A'$, which had a troughlike form joining the region between $R = 7.5\,a_0$, $\theta = 140°$ and $R = 8.0\,a_0$ and $\theta = 180°$. We also note that there is some confusion about the CH bond lengths employed in previous work. For example, Wagner *et al.* [19] mention the values of 2.1108 and 2.15 $a_0$, Cybulski *et al.* [21] used $r = 2.15\,a_0$ because they thought that that was the value employed by Wagner et al. Ben Abdallah *et al.* used 2.116 $a_0$ which is almost identical with the experimental value of 2.1163 $a_0$ (1.1199 Å) [23]. In a later work by Ben Abdallah et al. [24], inelastic cross sections were calculated using the PES from [22]. As the experiment provided only relative values of integral cross sections, Ben Abdallah *et al.* calculated the ratios of integral cross sections for transitions into $\Pi(A'')$ final levels over the ones into $\Pi(A')$ final levels. The discrepancy between theory and experiment was in most cases less than

7%, with worse agreement for transitions with larger inelasticity. Finally, Derouich and Ben Abdallah [25] used the PES from [22] to show that the coupled states (CS) approximation is sufficient for the photospheric conditions of the Sun but not for the interstellar medium where temperature is much lower.

In this work, we compute a new set of *ab initio* PESs for the ro-vibrational excitation of CH($X^2\Pi$) by He. Despite potential energy surfaces have been already published, this is the first set of PESs for this van der Waals complex computed using coupled clusters theory, which is a current state-of-the-art method for computing high quality potentials. Such PESs are highly needed in order to interpret past and future experiments on the inelastic scattering of CH with He. This paper is organized as follows: Section II presents the *ab initio* calculations, and the analytical fit of the PES obtained. In Section III, a comparison between experimental and theoretical inelastic ICS, DCS and rate coefficients is described. Conclusions drawn from this comparison, and future outlook are also presented.

## II. CONSTRUCTION AND FIT OF THE CH(X)–HE PES

### A. *Ab initio* calculations

As mentioned in the introduction, when the CH($X^2\Pi$) radical interacts with a spherical structureless target, the doubly-degenerate $\Pi$ electronic state is split into two states, one of $A'$ symmetry and one of $A''$ symmetry.

The CH–He "rigid rotor" PESs are described by the two Jacobi coordinates $R$, the distance from the centre of mass of CH molecule to the He atom, and $\theta$, the angle between $\vec{R}$ and the CH bond axis $\vec{r}$, with $\theta = 0°$ corresponding to collinear He–C–H.

The intermolecular bond distance of CH was frozen at its experimental equilibrium values [$r_{\rm CH} = 2.116$ bohr]. As demonstrated by Kalugina *et al.* [26], for the OH–He system, there may be slight differences between the two-dimensional PESs (calculated for a frozen bond distance) and the full dimensional PESs (obtained by averaging over the intermolecular ground state vibrational wavefunction). Consequently, in the present case, we anticipate that restricting the intramolecular distance to its equilibrium value may introduce little error into the calculated inelastic rate coefficients at low temperature. However, we expect that the inaccuracies will remain lower than the error bar of the experimental measurements or of the astronomical observations.

*Ab initio* calculations of the PESs of CH($X^2\Pi$)-He van der Waals complexes being in $A'$ and $A''$ electronic states were carried out at the partially spin-restricted coupled cluster with single, double and perturbative triple excitations [RCCSD(T)] [27, 28] level of theory using MOLPRO 2010 package [29]. In order to determine the interaction potential, $V(R, \theta, r_{\rm CH})$, the basis set superposition error (BSSE) was corrected at all geometries using the Boys and Bernardi counterpoise scheme [30]:

$$V(R,\theta,r_{\rm CH}) = E_{\rm CH-He}(R,\theta,r_{\rm CH}) - E_{\rm CH}(R,\theta,r_{\rm CH}) - E_{\rm He}(R,\theta,r_{\rm CH}) \quad (2)$$

where the energies of the CH and He monomers are computed in a full basis set of the complex.

For all three atoms, we used the standard correlation-consistent polarized valence-quadruple-zeta basis sets of Dunning [31] (cc-pVQZ) augmented with the diffuse functions of $s$, $p$, $d$, $f$ and $g$ symmetries (aug-cc-pVQZ) [32]. This basis set was further augmented by the [$3s3p2d2f1g$] bond functions optimized in Ref. [33] and placed at mid-distance between the He atom and the CH centre of mass.

The calculations were carried out for $\theta$ angle values from 0° to 180° in steps of 15°. $R$-distances were varied from 3.0 to 50.0 $a_0$, yielding 41 points for each angular orientation.

### B. Analytical representations

In order to perform the scattering calculations we need to represent the CH–He potentials in the form of analytical expressions. For this purpose, we expand the so-called half-sum ($V_{\rm sum}$) and half-difference ($V_{\rm diff}$) diabatic potentials, as previously defined by [16], in a series of reduced Wigner functions $d_{l\mu}(\cos\theta)$:

$$V_{\rm sum}(R,\theta) = \frac{1}{2}\left[V_{A''}(R,\theta) + V_{A'}(R,\theta)\right] = \sum_{l=0}^{l_{max}} V_{l0}(R) d_{l0}(\cos\theta) \quad (3)$$

$$V_{\rm diff}(R,\theta) = \frac{1}{2}\left[V_{A''}(R,\theta) - V_{A'}(R,\theta)\right] = \sum_{l=2}^{l_{max}} V_{l2}(R) d_{l2}(\cos\theta)\,. \quad (4)$$

For all the potentials in this work, we set $l_{max} = 12$. This ensures that the anisotropy of these potentials is well represented. The contour plots of our new $V_{\rm sum}$ and $V_{\rm diff}$ diabatic and $A''$ and $A'$ adiabatic potentials are shown in Figure 1. We determined the $V_{l\mu}(R)$ ($\mu = 0, 2$) radial coefficients by linear least squares fitting of the angular expansion at each discrete radial point to a set of angular *ab initio* points. The highly repulsive energies were weighted in the fit with a weight of $1/E^6$ to influence better description of the potential in the energies that will be sampled during the scattering process. The relative errors of the fits for typical distances are very small for both complexes (from 0.1 to $10^{-3}$ %). The absolute error in the region of the attractive long range interaction is usually on the order of $10^{-1}$ to $10^{-3}$ cm$^{-1}$ or better. The radial expansion coefficients $V_{l\mu}(R)$ obtained

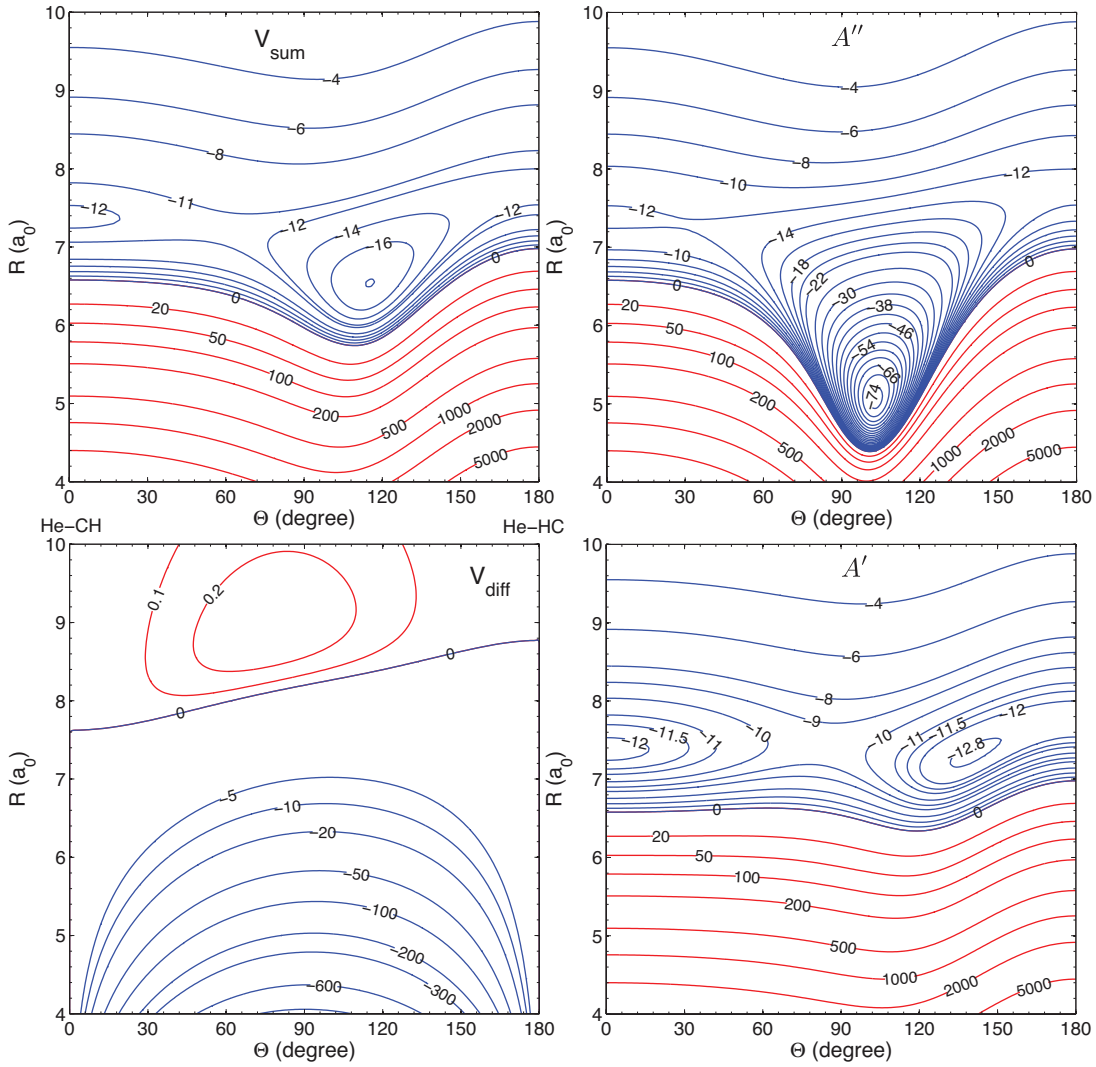


FIG. 1: Contour plots of CH(X)–He diabatic $V_{\rm sum}$ (upper left panel), and $V_{\rm diff}$ (lower left panel) RCCSD(T) potentials, and adiabatic $A''$ (upper right panel), and $A'$ (lower right panel) RCCSD(T) potentials from this work. Energy is in cm$^{-1}$. Red contour lines represent repulsive interaction energies.

in this way are then represented by the one-dimensional Reproducing Kernel Hilbert Space (RKHS) interpolation fits [34] with the smoothness parameter $m = 2$ and with the fixed long range $R^{-6}$ radial kernel for the extrapolation beyond the last *ab initio* radial point at $50\,a_0$. Plots of the radial coefficients of the potential determined in this work and potentials of Ben Abdallah *et al.* [22] and Cybulski *et al.* [21] are shown in Figure 2. The Fortran routines for the newly developed PES are given as supplementary data to this article.

### C. Features of the PESs

We will now describe features of the CH–He PESs and compare our work with previous UMP2 potentials by Cybulski *et al.* [21] and CEPA-1 ones by Ben Abdallah *et al.* [22]. The minimum geometry parameters of our $A''$, $A'$ and $V_{\rm sum}$ PESs are shown in Table I and compared to previously published potentials that we have just mentioned. The global minima of our new PESs are approximately 20% deeper than those by Ben Abdallah *et al.* and are even deeper than the results by Cybulski *et al.* This result is expected as we recover more correlation energy using the RCCSD(T) method than what CEPA-1 and UMP2 methods can provide. This effect can also be seen in the upper panel of Figure 2, where we show the isotropic $V_{00}(R)$ radial expansion coefficients; they are systematically more attractive when going from UMP2, through CEPA-1 to RCCSD(T) calculations. This means that we recover more of the dispersion energy described by the $C_6$ dispersion coefficient [35]. The other expansion coefficients for $l > 0$ are very similar between our PES and the one of Ben Abdallah *et al.* Those coefficients de-

scribe anisotropy of the PESs, which seems to be similar in these two PESs. The radial expansion coefficients of Cybulski *et al.* PESs, which are also shown in Figure 2, are distinctly different in comparison to present work or Ben Abdallah *et al.* One reason is that it originates from the UMP2 level of theory, and the second one, to a lesser extent, is that Cybulski *et al.* used slightly different CH diatomic distance in the determination of the PESs.

The $V_{\rm sum}$ diabatic potential shown in the upper left panel of Figure 1 is fairly shallow and characterized by the skewed T-shape global minimum and the local minimum for the He–C–H collinear geometry, whereas the collinear He–H–C geometry is a saddle point. The difference potential, shown in the lower left panel of Figure 1, is mostly described by the $V_{22}$ expansion term (see Figure 2) as it is pretty much symmetric with respect to $\theta = 90°$.

In the right column of Figure 1 we show adiabatic RCCSD(T) potentials: the $A''$ with a deep van der Waals minimum of -75.44 cm$^{-1}$ in the upper right panel, and the fairly isotropic $A'$ adiabat in the lower right panel. We refer the reader for the discussion of differences between the $A'$ and $A''$ PESs (with respect to anisotropy) to the detailed description by Cybulski *et al.* [21], where they partition the interaction energy into the perturbation theory components that can give clear insight into the potential's anisotropy. We believe that with the current combination of the state-of-the-art *ab initio* methodology with fairly large basis set and midbond functions our new potentials improve upon previously published potentials, giving more precise description of the interaction strength in the He-CH(X) van der Waals complex. This is important in scattering calculations for obtaining good quality collisional rate coefficients for astrophysical applications. We will now describe the scattering methodology.

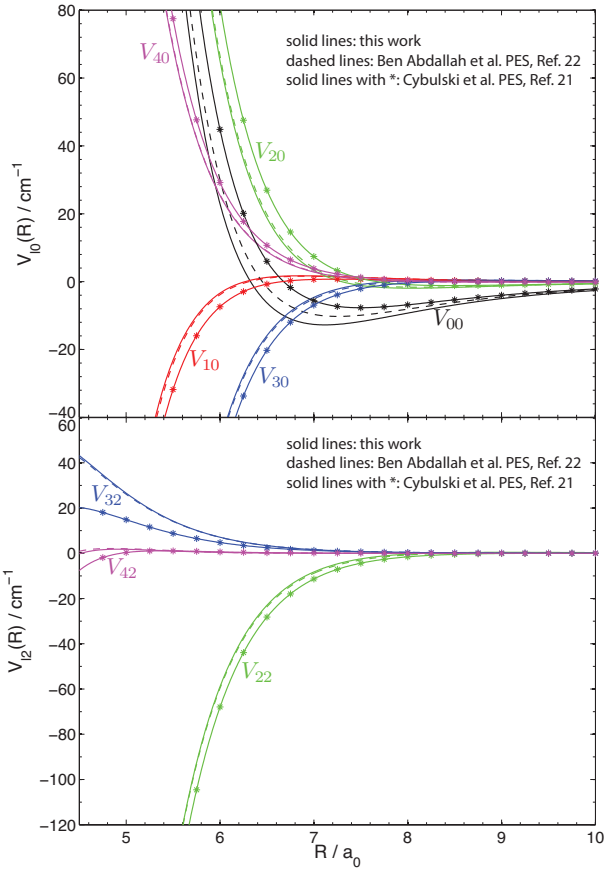


FIG. 2: Plots of the radial expansion coefficients of the He-CH(X) PESs: $V_{l0}$ defined in Eq. 3 (upper panel) and $V_{l2}$ defined in Eq. 4 (lower panel).

## III. RESULTS

### A. Scattering calculations

In order to test the newly constructed PES with available experimental data, close-coupling quantum scattering calculations were performed. The close-coupling calculations were carried out using HIBRIDON program [36], which provided integral and differential cross sections. The CH rotation, spin-orbit coupling and Λ-doublet splitting were taken into account, using for $v = 0$ the CH rotation constant $B = 14.1924\,\mathrm{cm}^{-1}$, the spin-orbit coupling constant $A = 28.1468\,\mathrm{cm}^{-1}$, and Λ-doubling parameters $p = 0.0335\,\mathrm{cm}^{-1}$ and $q = 0.0387\,\mathrm{cm}^{-1}$ [13]. In the scattering calculations reported here, the hyperfine structure of CH(X) was not taken into account, and the value of the spin-orbit constant was assumed to be independent of the CH–He intermolecular separation. The latter approximation is commonly employed in scattering calculations because of the moderate-to-large intermolecular separations at typical collision energies. The calculations were performed for collision energies up to $2500\,\mathrm{cm}^{-1}$, and a maximum value of total angular momentum ($J_{\rm tot} = 200$) and a maximum value of the rotational quantum number of the CH molecule ($J = 23$) were used.

### B. Integral Cross Sections

Integral cross sections were obtained for transitions up to $7.5fF_2$ and $8.5fF_1$ and for $E_{\rm col}$ up to $2500\,\mathrm{cm}^{-1}$. In crossed molecular beam experiments, it is difficult to obtain absolute values of integral cross sections. For this reason, previous experimental and theoretical work presented values of the ratio of integral cross sections into $A''$ final levels versus those into $A'$ final levels. A comparison between ratios calculated from this study and all previously published ratios are collated in Table II. The agreement between this study and previous computational work is reasonable given that this work used a more accurate PES. The results from this work reproduce most of the experimental data within the experimental error especially when we averaged over the initial experi-

TABLE I: Minimum geometries $(R_e, \theta_e)$ in bohr and degrees and minimum energies, $D_e$, in $\mathrm{cm}^{-1}$ for the He–CH($X^2\Pi$) $A''$, $A'$ and $V_{\mathrm{sum}}$ PESs calculated in this work and compared to previous published PESs. Note that Ben Abdallah's PES has an opposite definition of $\theta = 0$ which corresponds to the He-HC collinear geometry. Here we adjust the Jacobi angle to coincide with our definition of $\theta$. The additional entry in parenthesis for the $A'$ PES of Cybulski *et al.* shows equivalent skewed local minimum, which in our case and in Ben Abdallah's PES is a global minimum.

| Method | $R_e(A'')$ | $\theta_e(A'')$ | $D_e(A'')$ | $R_e(A')$ | $\theta_e(A')$ | $D_e(A')$ | $R_e(V_{\mathrm{sum}})$ | $\theta_e(V_{\mathrm{sum}})$ | $D_e(V_{\mathrm{sum}})$ |
|---|---|---|---|---|---|---|---|---|---|
| RCCSD(T)[a] | 5.06 | 103 | 75.44 | 7.32 | 140 | 12.94 | 6.56 | 116 | 18.03 |
| CEPA-1[b] | 5.16 | 103 | 61.56 | 7.44 | 141 | 10.50 | 6.76 | 117 | 14.23 |
| UMP2[c] | 5.26 | 103 | 50.74 | 7.74(7.71) | 0(138) | 7.72(7.64) | 6.99 | 116 | 10.64 |

[a] This work
[b] Ben Abdallah *et al.* PES [22]
[c] Cybulski *et al.* PES [21]

mental populations as provided by Alexander *et al.* [20]. The agreement between the experimental and theoretical values of the ratios is not that good for the $4.5F_2$ and $5.5F_2$ products. This could be explained if one considers that the initial (experimental) CH beam contained CH molecules in $N > 10$ which could contribute significantly in the creation of products. In addition, the population of the $4.5F_2$ and $5.5F_2$ products is low, and we can expect larger error for the measurements. It may also indicate that perhaps further improvement of the *ab initio* potential energy surfaces is possible, especially at short intermolecular separations which are expected to lead to products with high $N$.

Following Alexander *et al.* [20], we compare theoretical values of ICS and scaled experimental values at various collision energies in Fig. 3. The calculations have taken into account the initial (experimental) rotational populations as presented in the Table I by Alexander *et al.* [20]. The experimental values were taken from Fig. 4 in Ref. [20], and were scaled to the theoretical values by multiplication by a single constant factor. The comparison between theory and experiment is quantitative with few exceptions at very low or very high collision energies.

Most of the crossed molecular beam experiments are performed at collision energies around $500\,\mathrm{cm}^{-1}$. For this reason, the cross sections at that $E_{\mathrm{col}}$ for all possible inelastic transitions out of CH $(\mathrm{X}^2\Pi_{1/2}, v = 0, j = 0.5)$ + He collisions are shown in Fig. 4. Comparing the graphs in the lower panel with those in the upper panel, a propensity for spin-orbit manifold conserving $(F_2 \to F_2)$ transitions over spin-orbit manifold changing $(F_2 \to F_1)$ transitions is not observed. Alexander and Dagdigian observed such a propensity in CH(X) + Ar collisions [37]. The authors stated that purely electrostatic interactions can change only **N** but not **S**. Thus, the relative orientation of **N** and **S**, which determines the spin-orbit manifold, will have a propensity to remain the same during a collision. This propensity is observd but only at higher collision energies, as shown in Fig. 5. Such effect was also observed in OH(X)–He collisions [26, 38]. Comparing the ICS for transitions into $A''$ versus those into

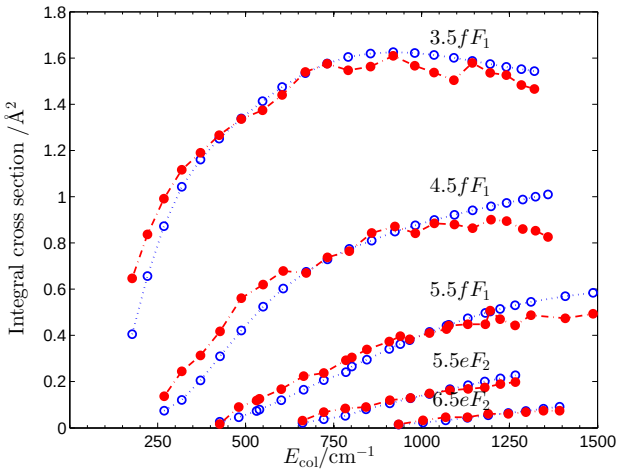


FIG. 3: Comparison of normalized experimental (filled red circles) and theoretical (empty blue circles) inelastic integral cross sections for transitions into specific CH Λ-doublet levels as a function of collision energy. The theoretical ICS were averaged over the experimentally measured initial populations [20]. The experimental ICS were scaled to the theoretical values. The final levels are indicated above the curves.

$A'$ levels, there is a propensity for transitions into the antisymmetric levels. This propensity appears in the ICS at various collision energies for final levels with $N > 5$, as shown in Fig. 5. We note that this propensity becomes less dominant and sometimes reverses at low $N$ levels. This happens because the degree of electron alignment strongly depends on the rotational level as shown in [17].

### C. Differential Cross Sections

The calculated DCSs were obtained with resolution of 1°. The full set of CH$(\mathrm{X}^2\Pi_{1/2}, v = 0, J = 0.5)$ +

TABLE II: Cross sections (in Å$^2$) for collisions out of CH($X^2\Pi_{1/2}, v = 0, J = 1/2$) + He at a collision energy of $1000\,\mathrm{cm}^{-1}$.

| Final state | | | | | | $(\sigma_{A''}/\sigma_{A'})$ | |
|---|---|---|---|---|---|---|---|
| $J'$ | $F_i'$ | $e \to e$ | $f \to f$ | $e \to f$ | $f \to e$ | Calc. | Expt. |
| 3/2 | 1 | 0.344 | 0.346 | 6.665 | 3.454 | 1.85[a] (1.63[b]) | ··· |
| 3/2 | 1 | | | | | 1.29[c] | |
| 3/2 | 1 | 0.4428 | 0.4291 | 6.203 | 3.667 | 1.61[d] (1.20[e]) | |
| 5/2 | 1 | 1.341 | 4.205 | 0.961 | 0.837 | 2.37[a] (2.15[b]) | ··· |
| 5/2 | 1 | | | | | 2.07[c] | |
| 5/2 | 1 | 1.350 | 4.145 | 0.7997 | 0.7246 | 2.38[d] (1.84[e]) | |
| 7/2 | 1 | 0.363 | 0.682 | 2.561 | 0.776 | 2.85[a] (2.44[b]) | 2.10[f] |
| 7/2 | 1 | | | | | 2.17[c] | |
| 7/2 | 1 | 0.3362 | 0.6625 | 2.187 | 0.8060 | 2.49[d] (1.95[e]) | |
| 9/2 | 1 | 0.285 | 1.199 | 0.513 | 0.251 | 3.19[a] (2.98[b]) | 2.48[f] |
| 9/2 | 1 | | | | | 2.61[c] | |
| 9/2 | 1 | 0.3321 | 1.129 | 0.5176 | 0.2295 | 2.93[d] (2.39[e]) | |
| 11/2 | 1 | 0.086 | 0.191 | 0.460 | 0.106 | 3.39[a] | 2.67[f] |
| 11/2 | 1 | 0.0932 | 0.2161 | 0.5296 | 0.1202 | 3.49[d] (2.78[e]) | |
| 3/2 | 2 | 0.317 | 0.308 | 3.631 | 7.075 | 1.88[a] (1.81[b]) | ··· |
| 3/2 | 2 | | | | | 1.80[c] | |
| 3/2 | 2 | 0.395 | 0.3917 | 3.130 | 6.449 | 1.94[d] (1.69[e]) | |
| 5/2 | 2 | 3.081 | 1.386 | 0.574 | 0.861 | 2.01[a] (1.96[b]) | 1.96[f] |
| 5/2 | 2 | 3.235 | 1.419 | 0.4776 | 0.7626 | 2.11[d] (1.90[e]) | |
| 7/2 | 2 | 0.418 | 0.121 | 0.520 | 1.766 | 3.41[a] (3.29[b]) | 1.91[f] |
| 7/2 | 2 | | | | | 2.55[c] | |
| 7/2 | 2 | 0.381 | 0.1347 | 0.6001 | 1.586 | 2.68[d] (2.35[e]) | |
| 9/2 | 2 | 0.494 | 0.112 | 0.069 | 0.165 | 3.64[a] | 2.31[f] |
| 9/2 | 2 | 0.5621 | 0.1496 | 0.07694 | 0.2062 | 3.39[d] (2.86[e]) | |
| 11/2 | 2 | 0.102 | 0.015 | 0.022 | 0.110 | 5.73[a] | 2.85[f] |
| 11/2 | 2 | 0.1137 | 0.01856 | 0.02886 | 0.1562 | 5.69[d] (3.90[e]) | |

[a] From Dagdigian *et al.* [18] using the Wagner-Dunning-Kok PES [19].
[b] Averaged values presented by Ben Abdallah *et al.* [24] based on initial values by Dagdigian *et al.* [18] using the Wagner-Dunning-Kok PES [19].
[c] From Ben Abdallah *et al.* [24] using the PES from Ben Abdallah *et al.* [22].
[d] This work using the newly constructed PES.
[e] This work using the newly constructed PES and averaging over the experimental initial populations taken from Alexander *et al.* [20].
[f] Values presented by Dagdigian *et al.* [18] using the experimental values by Macdonald *et al.* [17]. The experimental uncertainty was stated ±15%.

He DCSs for inelastic transitions at a collision energy of $500\,\mathrm{cm}^{-1}$, which is typical in molecular beam experiments, are shown in Fig. 6 for the 12 lowest energy levels in increasing energy of the final level. Using classical arguments, backward scattering is associated with sampling of the short-range repulsive potential, leading to transitions with high $\Delta J$. Generally, the theoretical results reproduce this trend. Another conclusion from Fig. 6 is that DCS into $A''$ final levels, i.e. $fF_1$ and $eF_2$ are more forward than into $A'$ final levels, i.e. $eF_1$ and $fF_2$. This is consistent with the argument by Dagdigian *et al.* [18] that the $A''$ surface is more attractive for a molecule of $\pi$ electron occupancy as the sole $\pi$ electron lies perpendicular to the triatomic plane.

Macdonald and Liu [17] had predicted the existence of rotational rainbows (i.e. maxima) in the DCSs based on (a) the dynamical threshold in the excitation functions, and (b) the distinct structures in the rotational level distributions at a fixed $E_{\mathrm{col}}$. Here we show that this system will show rotational rainbows in a typical crossed beam

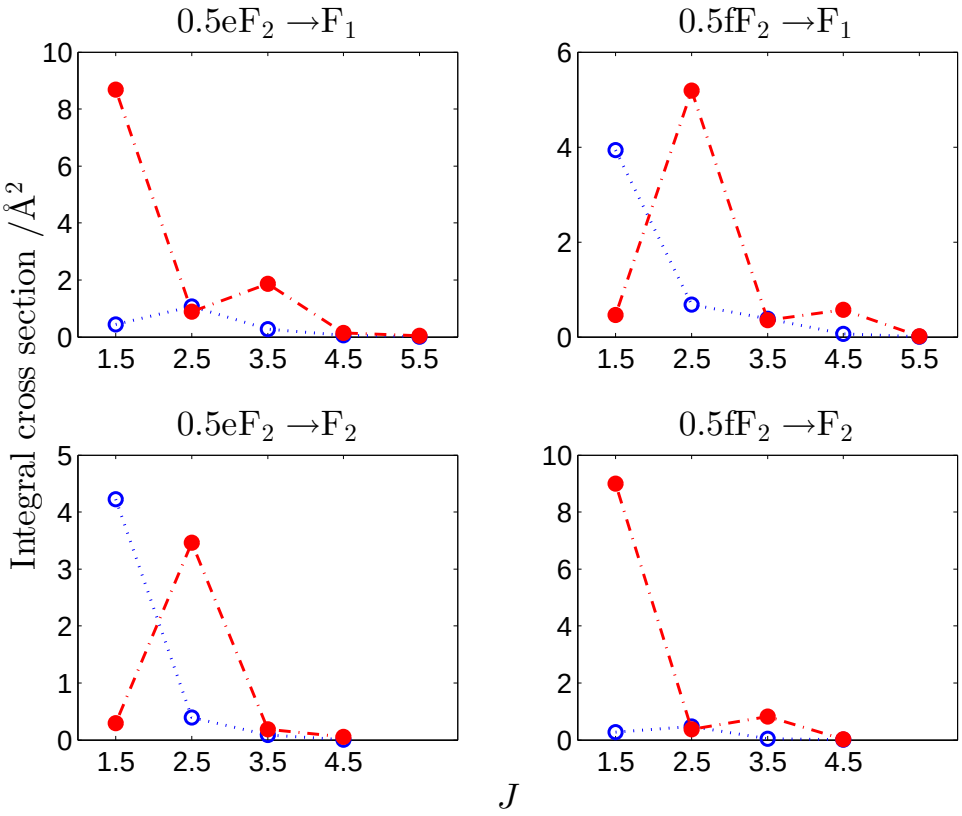


FIG. 4: State-to-state inelastic cross sections for CH ($X^2\Pi_{1/2}, v = 0, j = 0.5$) scattered by He at a collision energy of 500 $cm^{-1}$. The initial spin-orbit manifold and Λ-doublet symmetry, and the final spin-orbit manifold are indicated in the title of the graphs, the final $J$ quantum number is indicated on the abscissa. Transitions into $A''$ ($fF_1$ and $eF_2$) levels are represented by filled red circles; transitions into $A'$ ($eF_1$ and $fF_2$) levels are represented by empty blue circles.

experiment. Finding rotational rainbows in DCS is not always straightforward because, in most of the experiments, the initial population is an equal mixture of $e$ and $f$ levels. As shown in Fig. 6, rotational rainbows will be easier observed if we select the initial Λ-doublet level. As it is currently possible to select only $f$ initial levels using hexapole field [39], we propose a DCS experimental measurement for the transition $0.5fF_2 \rightarrow 3.5fF_2$. If it was possible to select $e$ initial levels, we would propose a DCS experimental measurement for the transitions $0.5eF_2 \rightarrow 2.5eF_1, 3.5eF_1$.

### D. Kinetic Rate Coefficients

Thermal rate coefficients were obtained by integration of the integral cross sections over a Boltzmann distribution of relative translational energies using a reduced mass $\mu = 3.0608$ amu. Rate coefficients were calculated for temperatures between 10 and 300 K. The complete set of (de)excitation rate coefficients among 31 channels (up to $7.5fF_2$ and up to $8.5fF_1$) will be available online from the BASECOL database [40]. In Fig. 7, the rate coefficients for the same transitions as those in Fig. 5 are shown. A clear observation from Fig. 7 is that the propensity for transitions into final $A''$ levels becomes more pronounced at higher temperatures.

Due to the low density of the interstellar medium, the energy levels of the molecules are not at local thermodynamical equilibrium. Thus modelling of molecular emission of these species requires excitation calculations using radiative as well as collisional rate coefficients with the most abundant interstellar species that are generally He and $H_2$. The present rate coefficients, the first published for the CH molecule, will allow to perform model calculations with the goal to fit the observational data available in the Herschel archive and/or future observations of the CH molecule. Hence, it will be possible to have an accurate estimation of the CH abundance in molecular clouds.

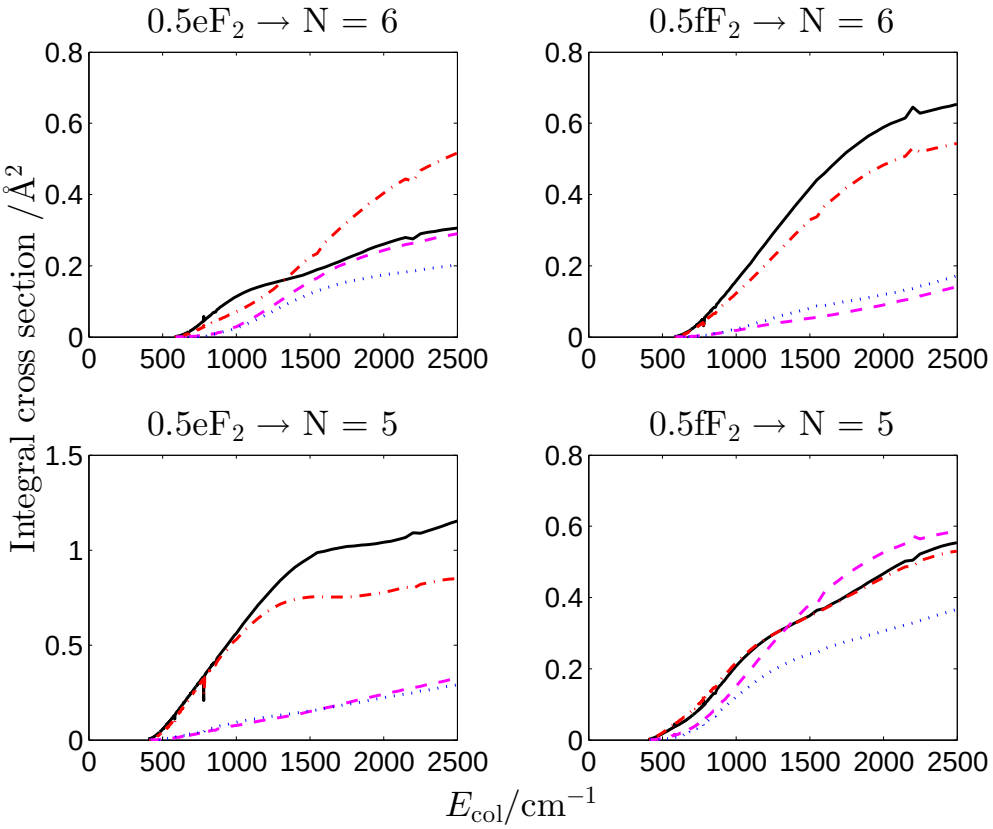


FIG. 5: State-to-state excitation functions for CH ($X^2\Pi_{1/2}, v = 0, j = 0.5$) scattered by He. The final $N$ quantum number is shown in the title of the graphs. The final products are shown: $eF_2$ (black solid), $fF_2$ (purple dashed), $eF_1$ (blue dotted) and $fF_1$ (red dashed-dotted).

## IV. DISCUSSION

In summary, the quality of the new, two dimensional CH(X)-He PES is verified by comparison with previous experimental and theoretical data. The results from this computational work show the best agreement with the available experimental values. We also showed that future measurements of DCS will exhibit rotational rainbows if the initial Λ-doublet level is selected using hexapole field. We verified the previously observed propensity for population of $\Pi(A'')$ final levels in rotational excitation of CH(X) radicals by He, and we showed for the first time that this propensity will also be observed in rate coefficients and magnified at higher temperatures.

The CH(X)-He rate coefficients, presented here for the first time, can be used to aid astrophysical modelling. Accurately determining the CH abundance in the interstellar medium is of key importance. Indeed, the CH radical is highly reactive and the reaction of CH with the different interstellar atoms (O, N, C) will contribute to initiate the interstellar chemistry. In particular, the reaction of CH with atomic N or C will be major sources of key interstellar molecules like CN or $C_2$ [41]. We then anticipate significant advances in the interstellar (carbon) chemistry understanding by the use of these new collisional data.

New CH(X) + He scattering experiments will be soon started within the HYDRIDES project [42] In these experiments, inelastic rate coefficients for CH(X) collisions at low and intermediate temperatures will be measured. The present data will allow full analysis of the experimental measurement. Finally, the extension of this work to collisions of CH radicals with other collision partners (H, $H_2$, rare gas) will provide valuable information in a rich variety of chemical processes where the CH is a key species.

## ACKNOWLEDGEMENTS

S. M. and F. L. greatly acknowledge the financial support of ANR project 'HYDRIDES'. This research utilized Queen Mary's MidPlus computational facilities, supported by QMUL Research-IT and funded by EPSRC grant EP/K000128/1. J. K. acknowledges the financial support by the National Science Foundation Grant No. CHE-1213332 to M. H. Alexander. S. M. acknowledges Dr Ben Abdallah for very useful discussions.

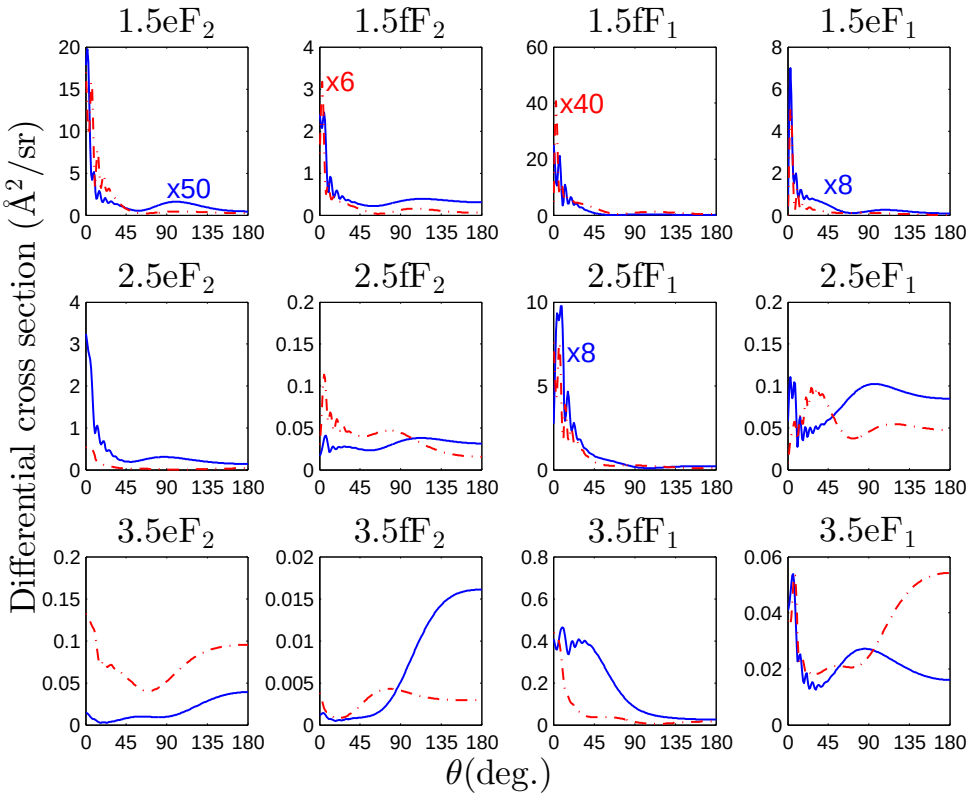


FIG. 6: Close-coupling quantum mechanical differential cross sections (DCSs) for transitions out of CH(X $^2\Pi_{1/2}, v = 0, J = 0.5f$) + He at $E_{\rm col} = 500\,{\rm cm}^{-1}$. The theoretical results obtained using the newly constructed PES are from this work. The final quantum numbers are shown in the title of the graphs. Transitions from $0.5eF_2$ and $0.5fF_2$ are represented by blue, solid lines and red, dashed-dotted lines, respectively.


[1] N. Peters and B. Rogg (editors), *Reduced kinetic mechanisms for appplications in combustion systems* (Springer-Verlag, Heidelberg, 1993).

[2] L. M. Ziurys and B. E. Turner, Astrophys. J. **292**, L25 (1985).

[3] C. E. Moore and H. P. Broida, J. Res. Nat. Bur. Stand. **63**, A19 (1959).

[4] T. Masseron, B. Plez, S. Van Eck, R. Colin, I. Daoutidis, M. Godefroid, P.-F. Coheur, P. Bernath, A. Jorissen, and N. Christlieb, A&A **571**, A47 (2014).

[5] D. A. Mendis and W.-H. Ip, Astrophys. Space Sci. **39**, 335 (1976).

[6] M. H. D. van der Wiel, F. F. S. van der Tak, D. C. Lis, T. Bell, E. A. Bergin, C. Comito, M. Emprechtinger, P. Schilke, E. Caux, C. Ceccarelli, A. Baudry, P. F. Goldsmith, E. Herbst, W. Langer, S. Lord, D. Neufeld, J. Pearson, T. Phillips, R. Rolffs, H. Yorke, A. Bacmann, M. Benedettini, G. A. Blake, A. Boogert, S. Bottinelli, S. Cabrit, P. Caselli, A. Castets, J. Cernicharo, C. Codella, A. Coutens, N. Crimier, K. Demyk, C. Dominik, P. Encrenaz, E. Falgarone, A. Fuente, M. Gerin, F. Helmich, P. Hennebelle, T. Henning, P. Hily-Blant, T. Jacq, C. Kahane, M. Kama, A. Klotz, B. Lefloch, A. Lorenzani, S. Maret, G. Melnick, B. Nisini, S. Pacheco, L. Pagani, B. Parise, M. Salez, P. Saraceno, K. Schuster, A. G. G. M. Tielens, C. Vastel, S. Viti, V. Wakelam, A. Walters, F. Wyrowski, K. Edwards, J. Zmuidzinas, P. Morris, L. A. Samoska, and D. Teyssier, A&A **521**, L43 (2010).

[7] M. Gerin, M. de Luca, J. R. Goicoechea, E. Herbst, E. Falgarone, B. Godard, T. A. Bell, A. Coutens, M. Kaźmierczak, P. Sonnentrucker, J. H. Black, D. A. Neufeld, T. G. Phillips, and J. Pearson, A&A **521**, L16 (2010).

[8] S.-L. Qin, P. Schilke, C. Comito, T. Möller, R. Rolffs, H. S. P. Müller, A. Belloche, K. M. Menten, D. C. Lis, T. G. Phillips, E. A. Bergin, T. A. Bell, N. R. Crockett, G. A. Blake, S. Cabrit, E. Caux, C. Ceccarelli, J. Cernicharo, F. Daniel, M.-L. Dubernet, M. Emprechtinger, P. Encrenaz, E. Falgarone, M. Gerin, T. F. Giesen, J. R. Goicoechea, P. F. Goldsmith, H. Gupta, E. Herbst, C. Joblin, D. Johnstone, W. D. Langer, S. D. Lord, S. Maret, P. G. Martin, G. J. Melnick, P. Morris, J. A. Murphy, D. A. Neufeld, V. Ossenkopf, L. Pagani, J. C. Pearson, M. Pérault, R. Plume, M. Salez, S. Schlemmer, J. Stutzki, N. Trappe, F. F. S. van der

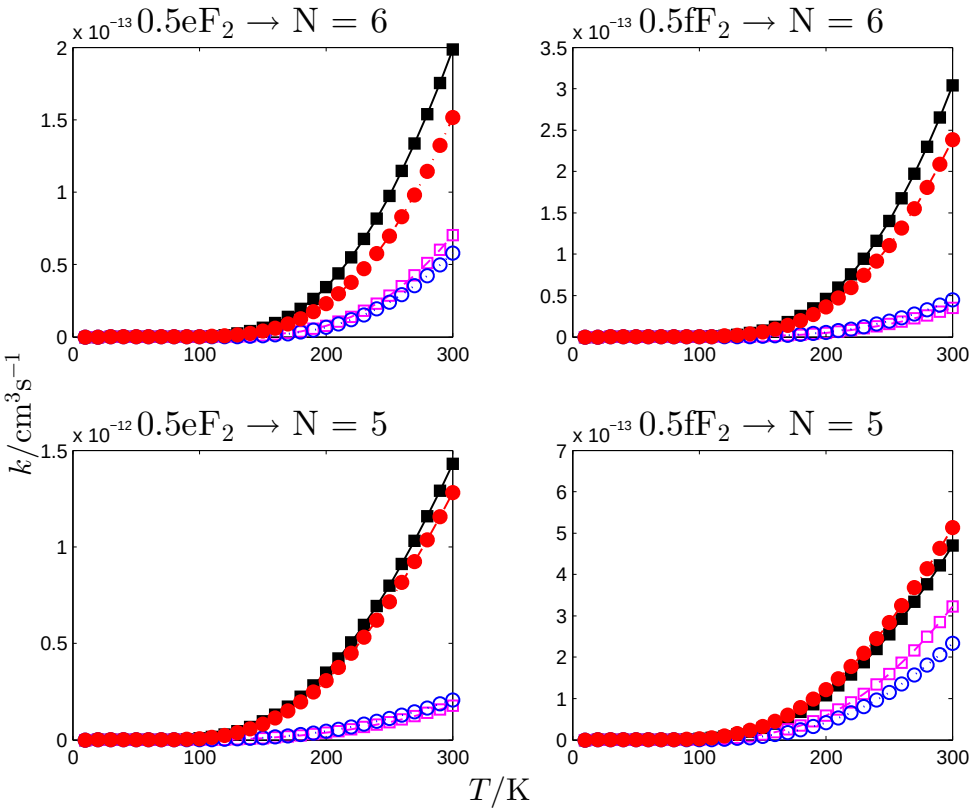


FIG. 7: Temperature dependence of state-to-state rate coefficients for transitions out of CH ($X^2\Pi_{1/2}, v = 0, j = 0.5$) + He. The final $N$ quantum number is shown in the title of the graphs. The final products are shown: $eF_2$ (black filled squares), $fF_2$ (purple open squares), $eF_1$ (blue open circles) and $fF_1$ (red filled circles).


Tak, C. Vastel, S. Wang, H. W. Yorke, S. Yu, J. Zmuidzinas, A. Boogert, R. Güsten, P. Hartogh, N. Honingh, A. Karpov, J. Kooi, J.-M. Krieg, R. Schieder, M. C. Diez-Gonzalez, R. Bachiller, J. Martin-Pintado, W. Baechtold, M. Olberg, L. H. Nordh, J. L. Gill, and G. Chattopadhyay, A&A **521**, L14 (2010).

[9] S. Truppe, R. J. Hendricks, S. K. Tokunaga, H. J. Lewandowski, M. G. Kozlov, C. Henkel, E. A. Hinds, and M. R. Tarbutt, Nat. Commun. **4**, 2600 (2013).

[10] S. Truppe, R. J. Hendricks, E. A. Hinds, and M. R. Tarbutt, J. Mol. Spectrosc. **300**, 70 (2014).

[11] S. Truppe, R. J. Hendricks, E. A. Hinds, and M. R. Tarbutt, Astrophys. J. **780**, 71 (2014).

[12] J. M. Brown and A. Carrington, *Rotational Spectroscopy of Diatomic Molecules* (Cambridge University Press, Cambridge, 2003).

[13] M. C. McCarthy, S. Mohamed, J. M. Brown, and P. Thaddeus, PNAS **103**, 12263 (2006).

[14] J. M. Brown, J. Hougen, K.-P. Huber, J. Johns, I. Kopp, H. Lefebvre-Brion, A. Merer, D. Ramsay, J. Rostas, and R. Zare, J. Molec. Spectrosc. **55**, 500 (1975).

[15] M. H. Alexander, P. Andresen, R. Bacis, R. Bersohn, F. J. Comes, P. J. Dagdigian, R. N. Dixon, R. W. Field, G. W. Flynn, K.-H. Gericke, E. R. Grant, B. J. Howard, J. R. Huber, D. S. King, J. L. Kinsey, K. Kleinermanns, K. Kuchitsu, A. C. Luntz, A. J. MacCaffery, B. Pouilly, H. Reisler, S. Rosenwaks, E. Rothe, M. Shapiro, J. P. Simons, R. Vasudev, J. R. Wiesenfeld, C. Wittig, , and R. N. Zare, J. Chem. Phys. **89**, 1749 (1988).

[16] M. Alexander, Chem. Phys. **92**, 337 (1985).

[17] R. Macdonald and K.Liu, J. Chem. Phys. **91**, 821 (1989).

[18] P. J. Dagdigian, M. H. Alexander, and K. Liu, J. Chem. Phys. **91**, 839 (1989).

[19] A. F. Wagner, T. H. Dunning, Jr., and R. A. Kok, J. Chem. Phys. **100**, 1326 (1994).

[20] M. H. Alexander, W. R. Kearney, and A. F. Wagner, J. Chem. Phys. **100**, 1338 (1994).

[21] S. M. Cybulski, G. Chałasiński, and M. M. Szczęśniak, J. Chem. Phys. **105**, 9525 (1996).

[22] D. Ben Abdallah, N. Jaidane, and Z. Ben Lakhdar, Phys. Chem. News **12**, 1 (2003).

[23] K. P. Huber and G. Herzberg, *Molecular Spectra and Molecular Structure. IV. Constants of Diatomic Molecules* (Van Nostrand Reinhold, New York, 1979).

[24] D. Ben Abdallah, N. Jaidane, Z. Ben Lakhdar, A. Spielfiedel, and N. Feautrier, J. Chem. Phys. **118**, 2003 (2003).

[25] M. Derouich and D. Ben Abdallah, in *Solar Polarization 5: In Honor of Jan Stenflo*, Astronomical Society of the Pacific Conference Series, Vol. 405, edited by S. V. Berdyugina, K. N. Nagendra, and R. Ramelli (2009) p. 355.

[26] Y. Kalugina, F. Lique, and S. Marinakis, Phys. Chem. Chem. Phys. **16**, 13500 (2014).

[27] C. Hampel, K. A. Peterson, and H.-J. Werner, Chem. Phys. Lett. **190**, 1 (1992).

[28] J. D. Watts, J. Gauss, and R. J. Bartlett, J. Chem. Phys. **98**, 8718 (1993).

[29] H.-J. Werner, P. J. Knowles, G. Knizia, F. R. Manby, M. Schütz, P. Celani, T. Korona, R. Lindh, A. Mitrushenkov, G. Rauhut, K. R. Shamasundar, T. B. Adler, R. D. Amos, A. Bernhardsson, A. Berning, D. L. Cooper, M. J. O. Deegan, A. J. Dobbyn, F. Eckert, E. Goll, C. Hampel, A. Hesselmann, G. Hetzer, T. Hrenar, G. Jansen, C. Köppl, Y. Liu, A. W. Lloyd, R. A. Mata, A. J. May, S. J. McNicholas, W. Meyer, M. E. Mura, A. Nicklass, D. P. O'Neill, P. Palmieri, K. Pflüger, R. Pitzer, M. Reiher, T. Shiozaki, H. Stoll, A. J. Stone, R. Tarroni, T. Thorsteinsson, M. Wang and A. Wolf, *MOLPRO*, *version 2010.1*, a package of *ab initio* programs, 2010, see http://www.molpro.net.

[30] S. F. Boys and F. Bernardi, Mol. Phys. **19**, 553 (1970).

[31] T. H. Dunning, J. Chem. Phys. **90**, 1007 (1989).

[32] R. A. Kendall, T. H. Dunning, and R. J. Harrison, J. Chem. Phys. **96**, 6796 (1992).

[33] S. M. Cybulski and R. Toczyłowski, J. Chem. Phys. **111**, 10520 (1999).

[34] T.-S. Ho and H. Rabitz, J. Chem. Phys. **104**, 2584 (1996).

[35] B. Jeziorski, R. Moszynski, and K. Szalewicz, Chem. Rev. **94**, 1887 (1994).

[36] The HIBRIDON package (version 4.4) was written by M. H. Alexander, D. E. Manolopoulos, H.-J. Werner, B. Follmeg, and P. Dagdigian with contributions by D. Lemoine, P. F. Vohralik, G. Corey, R. Gordon, B. Johnson, T. Orlikowski, A. Berning, A. Degli-Esposti, C. Rist, B. Pouilly, J. Kłos, Q. Ma, G. van der Sanden, M. Yang, F. de Weerd, S. Gregurick, and F. Lique, http://www2.chem.umd.edu/groups/alexander/.

[37] M. H. Alexander and P. J. Dagdigian, J. Chem. Phys. **101**, 7468 (1994).

[38] J. Kłos, F. Lique, and M. H. Alexander, Chem. Phys. Lett. **445**, 12 (2007).

[39] M. Brouard, D. H. Parker, and S. Y. T. van de Meerakker, Chem. Soc. Rev. **43**, 7279 (2014).

[40] Dubernet, M.-L., Alexander, M. H., Ba, Y. A., Balakrishnan, N., Balança, C., Ceccarelli, C., Cernicharo, J., Daniel, F., Dayou, F., Doronin, M., Dumouchel, F., Faure, A., Feautrier, N., Flower, D. R., Grosjean, A., Halvick, P., Kłos, J., Lique, F., McBane, G. C., Marinakis, S., Moreau, N., Moszynski, R., Neufeld, D. A., Roueff, E., Schilke, P., Spielfiedel, A., Stancil, P. C., Stoecklin, T., Tennyson, J., Yang, B., Vasserot, A.-M., and Wiesenfeld, L., A&A **553**, A50 (2013).

[41] I. W. M. Smith, E. Herbst, and Q. Chang, MNRAS **350**, 323 (2004).

[42] See http://ipag.osug.fr/Hydrides.